2025 IEEE 34st Microelectronics Design & Test Symposium (MDTS) | 979-8-3315-3689-3/25/$31.00 ©2025 IEEE | DOI: 10.1109/MDTS64924.2025.11177105

Microelectronics Differential Impedance Spectrometry System: Modeling and Noise Analysis for Biomedical Sensing Applications

Muhammad Nabeel Tahir
Department of Electrical and Computer Engineering
Rutgers, The State University of New Jersey
Piscataway, United States
nabeel.tahir@rutgers.edu

Umer Hassan*
Department of Electrical and Computer Engineering
Rutgers, The State University of New Jersey
Piscataway, United States
umer.hassan@rutgers.edu

***Abstract*—The need to diagnose complex and novel diseases has introduced significant advances in biosensing technologies, more specifically, miniaturized bio-electronics methods. Many of these diagnostic systems revolve around bioparticle quantification based on electrochemical impedance spectrometry (EIS). However, the robustness and accuracy of these systems still need improvement because of the nature of the electrical signals generated by the bioparticles, which are subject to a multitude of complex noise sources in microelectronics systems. Therefore, it is important to understand the behavior of different noise-introducing elements in the desired frequency bandwidth to better design the output signal detection and filtering circuits. Here, we modeled the microelectronics impedance spectrometry system and performed the noise simulations of two configurations of the EIS system. It was observed that for a microfluidic channel with an estimated resistance of $100k\Omega$, the feedback resistors introduce a noise of RMS $3mV$ in a dual-electrode configuration and a noise of RMS $7mV$ in a three-electrodes (differential) configuration in the bandwidth of 1THz. This information can be employed in designing effective noise-filtering circuits and selecting the operable bandwidth of the EIS system, as the system introduces noise in the order of a few hundred microvolts in the 3- 10 MHz frequency range.**

***Index Terms*—Electrochemical impedance spectrometry (EIS), input referred noise, differential impedance flow cytometer, and microfluidic.**

I. Introduction

Electrochemical impedance spectrometry (EIS) has been employed as an efficient tool in biomedical and diagnostic applications as it can provide critical information regarding the functioning of the immune system [1], the status of particular diseases [2], and the effectiveness of administered drugs [3]. The EIS system records the electrical signals (analogous to a change in impedance) for each type of bio-particle when it passes through a narrow microfluidic channel. This electrical information can be used to enumerate a particular population of bio-particles. A significant amount of research has been conducted to employ EIS to quantify cells and analyze the particle sizes [4] and to diagnose complex diseases, e.g., sepsis, Parkinson's, respiratory diseases, and study bladder pathology [5]–[8]. To realize these applications of EIS, various architectures have been developed and explored, ranging from two electrode-based systems to multi-electrode-based co-planer, circular, or 3D systems [4], [9]–[11]. Our group has also developed three electrode-based differential impedance cytometry systems for the quantification of white blood cells for various diagnostic applications [12], [13]. The microfluidic components of an EIS system can be modeled as electrical components to analyze the system's behavior. Like any electrical system, the EIS system is subject to noise from all the elements in the detection circuitry [14]. As the system measures the change in impedance as a cell passes through a microfluidic channel, the detection signal can be highly corrupted by the system noise and produce erroneous readings [10], [15]. Therefore, it is necessary to completely understand and study the effect of different circuit elements on the system's output. Previous studies have tried to explore the noise considerations of EIS systems, but were limited to output noise and simpler architectures of EIS [15]–[17]. The

*Corresponding Author
Work is supported by the U.S. National Science Foundation (Award No. 2329761).

understanding of the noise floor and the contribution of each circuit element are crucial in designing the right filters and selecting the frequency bandwidth of operations for the EIS system. Hence, the analysis and contribution of individual elements to the input and output noise of the EIS system are required.

In this study, we present the noise analysis of the two configurations of the EIS system, including the contribution of different elements using simulations and analytical results. The total input and output noise signatures in a two-electrode EIS system where one electrode is used as input for acquiring the signal are analytically calculated and compared with simulated results. The analysis is extended to three electrode systems where differential signals are measured. This noise analysis can be adapted to the other configurations of the EIS and used to develop low noise and robust detection systems. The rest of the paper is organized into a methods and materials section that provides analytical calculations and a results section that compares the simulated and calculated results.

II. Methods and Material

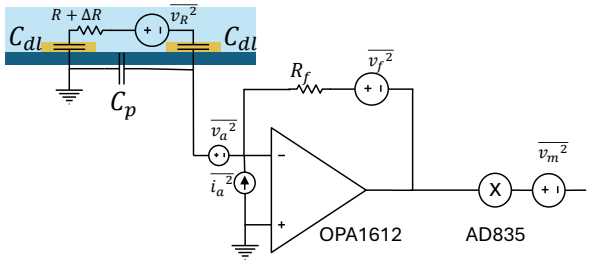

Fig. 1: Dual electrode impedance spectrometry (lock-in amplifier) equivalent circuit model with noise sources.

The EIS system presented in this study builds on the architectures presented in [16] and [13]. The system consists of an ultra-low noise OPA1612 operational amplifier and AD835, as well as a low-noise voltage mixer to create the lock-in amplifier circuit. The modeled microfluidic channel consists of gold electrodes of width and length of $100\mu m$ each, with a spacing between electrodes of $150\mu m$ and height of the channel $22\mu m$.

A. Modeling of Dual Electrode EIS System

Input referred current noise of this EIS system can be calculated as the sum of the current noise from all the sources mentioned below.

$$\overline{I_{in}}^2 = \overline{I_R}^2 + \overline{I_{a(v)}}^2 + \overline{I_a}^2 + \overline{I_f}^2 + \overline{I_m}^2 \quad (1)$$

Where $\overline{I_{in}}^2$ represents the input referred to as total current noise, $\overline{I_R}^2$ Nyquist or thermal noise current of equivalent resistance of the solution, $\overline{I_{a\ (v)}}^2 the$ noise current due to the voltage noise of the amplifier, $\overline{I_a}^2$ current noise of the amplifier, $\overline{I_f}^2$ thermal noise current of the feedback resistor, and $\overline{I_m}^2$ current noise of the mixer,as shown in the Fig. 1. Using the superposition principle, we can calculate the total input referred current as:

$$\overline{I_{in}}^2 = \frac{\overline{v_R^2}}{\|\frac{1}{j\omega C_{dl}} + R\|^2} + \frac{\overline{v_a^2}}{\|\frac{1}{j\omega C_{dl}} + R\|^2} + \overline{I_a^2} + \frac{\overline{v_f^2}}{R_f^2} + \frac{\overline{v_m^2}}{R_f^2} \quad (2)$$

$$\overline{v_{in}}^2 = \overline{I_{in}}^2 \times \|\frac{1}{j\omega C_{dl}} + R\|^2 \quad (3)$$

One can estimate the C_{dl} by using the per-unit length estimate of C_{dl} of the electrodes. The C_{dl} of gold electrodes is estimated to be in range $1-5\ \mu F/cm^2$ [18]. Using this information, the double layer capacitance of the gold electrodes having a width (w), and length (l) of $100\ \mu m$ respectively can be calculated as.

$$C_{dl} = 1 \times 10^{-6} \times 10^{-4} \left(\frac{F}{m^2}\right) \times 100 \times 10^{-6} \times 100 \times 10^{-6} m^2 = 0.1nF \quad (4)$$

and ΔR that represents the change in the resistance when a cell passes through a microfluidic channel, it can be calculated [19].

$$\Delta R = \frac{4\rho d^3}{\pi D^4} \quad (5)$$

Where, ρ represents the resistivity of the electrolyte, d diameter if the passing cell, and D the effective diameter of the channel. Similarly, the resistance offered by the microfluidic channel of length L filled with a fluid of resistivity ρ can be calculated as.

$$R = \frac{4\rho L}{\pi D^2} \quad (6)$$

For the rectangular channel, the effective diameter can be calculated as.

$$D = \frac{2hl}{h+l} = \frac{2(22 \times 10^{-6} \times 100 \times 10^{-6})}{22 \times 10^{-6} + 100 \times 10^{-6}} = 3.6 \times 10^{-5} m \quad (7)$$

The phosphate buffer saline solution (PBS) used as an electrolyte has a resistivity of $\rho = 0.7\Omega m$, and for a cell

with a diameter of $10\mu m$ the change in the resistance can be calculated as.

$$R + \Delta R = \frac{4\rho L}{\pi D^2} + \frac{4\rho d^3}{\pi D^4} \approx 100k\Omega \tag{8}$$

Using this information, the cutoff frequency can be calculated as.

$$f > \frac{1}{\pi(R + \Delta R)C_{dl}} \rightarrow f > 32kHz \tag{9}$$

The voltage noise of the solution resistance, amplifier, and feedback resistance can be calculated using equations.

$$\overline{v_R{}^2} = 4kT(R + \Delta R)\Delta f \tag{10}$$

$$\overline{v_f{}^2} = 4kT(R_f)\Delta f \tag{11}$$

In above equations k is Botlzman constant, T is temperature, R_f is feedback resistance while, Δf represents the frequency bandwidth. Assuming a bandwidth of $1MHz$ and $R_f = 1M\Omega$ for the gain the of 10 results in $\overline{v_R{}^2} = 1.656 \times 10^{-9}V^2$ and $\overline{v_f{}^2} = 1.656 \times 10^{-8}V^2$.

Knowing voltage mixer noise as $1nV/\sqrt{Hz}$, voltage noise of LPF, $2nV/\sqrt{Hz}$, input-referred current noise density of the amplifier as $1.7pA/\sqrt{Hz}$, input voltage voltage noise density as $1.1nV/\sqrt{Hz}$. We can calculate the total current noise value as.

$$\overline{I_{in}{}^2} = \frac{1.656 \times 10^{-9}v^2}{(100k)^2} + \frac{1.1 \times 10^{-9}v^2}{(100k)^2} + (1.7 \times 10^{-12})^2 \times 10^6 + \frac{1.656 \times 10^{-8}v^2}{(1M)^2} + \frac{(1 \times 10^{-9})^2 \times 10^6}{(1M)^2} + \frac{(2 \times 10^{-9})^2 \times 10^6}{(1M)^2}$$

$$\overline{I_{in}{}^2} = 2.92 \times 10^{-19}A^2 \tag{12}$$

$$\overline{v_{in}{}^2} = (100k)^2 \times 2.289 \times 10^{-19}A^2 = 2.92 \times 10^{-9}V^2 \tag{13}$$

At frequencies higher than $100kHz$ Z_{cdl} approaches zero, and the circuit behaves like an inverting operational amplifier with noise gains as:

$$A_n = 1 + \frac{R_f}{R + \Delta R} = 11 \tag{14}$$

The output noise can be calculated as:

$$\overline{v_o{}^2} = \overline{v_{in}{}^2} \times A_n^2 = 3.53 \times 10^{-7}V^2 \tag{15}$$

B. Modeling of Differential Electrode EIS System

The Fig. 2 shows the equivalent circuit of the differential impedance flow cytometer. The AC input of 10V is applied to the center electrode while the output is taken from the two side electrodes. The output signal is fed to trans-impedance current amplifiers with an effective gain of 10 through external resistors $R_{ext} = 10k\Omega$. As the input signal has a frequency higher than 100kHz, the double layer impedance acts as short-circuited, and the equivalent circuit essentially contains $R + \Delta R \approx R = 100k\Omega$ in series with R_{ext} while the other end connected to ground. Making the noise analysis simpler. Designing the two-stage amplifier circuit with gain at each stage of 10 results in the feedback resistor values of $R_{f1} = 1M\Omega$, $R_{f2} = 1k\Omega$ and noise gain of $A_{n,U1} = A_{n,U2} = 1 + \frac{R_{f1}}{R_{ext}+R} = 11$. The thermal noise contribution of the resistors $R_{f1}, R_{f2}, R_{ext}, and\ R$ can be calculated as:

$$\overline{v_{R_{ext}+R}{}^2} = 4kT(R_{ext}+R)\Delta f = 1.82\times10^{-9}V^2 \tag{16}$$

$$\overline{v_{R_{f1}}{}^2} = 4kT(R_{f1})\Delta f = 1.656 \times 10^{-8}V^2 \tag{17}$$

By calculating the voltage noise due to input referred current of the OpAmp as, $\overline{v_{i,U1}^2} = \overline{v_{i,U2}^2} = \overline{i_{U1}^2}(R_{f1}||(R_{ext}+R)^2 = 7.93 \times 10^{-9}V^2$ the total input noise voltage can be calculated:

$$\overline{v_{in,U1}^2} = \overline{v_{in,U2}^2} = \overline{v_{R_{ext}+R}{}^2}(\frac{R_{f1}}{R_{ext}+R+R_{f1}})^2 + \overline{v_{R_f}{}^2} (\frac{R_{ext}+R}{R_{ext}+R+R_{f1}})^2 + \overline{v_{i,U2}^2} + \overline{v_{U2}^2} = 9.41 \times 10^{-9}V^2 \tag{18}$$

The total output noise at the output terminal of the first-stage amplifiers can be obtained by multiplying the noise gain by the calculated input noise voltages.

$$\overline{v_{o,U1}{}^2} = \overline{v_{o,U2}{}^2} = \overline{v_{in,U1}^2} \times A_{n,U1}^2 = 1.13 \times 10^{-6}V^2 \tag{19}$$

Similarly, the contribution of the each resistive element and operational amplifier internal noise sources towards the output noise voltage of the second differential amplifier with a noise gain of $A_{n,U3} = \frac{R_1+R_{f2}}{R_1} = 2$ can be calculated as.

$$\overline{v_{o,R_{f2}}{}^2} = 4kT(R_{f2})\Delta f = 1.656 \times 10^{-14}V^2 \tag{20}$$

$$\overline{v_{o,R_1}{}^2} = 4kT(R_1)\Delta f(\frac{R_{f2}}{R_1})^2 = 1.656 \times 10^{-14}V^2 \tag{21}$$

$$\overline{v_{o,R_2}{}^2} = 4kT(R_2)\Delta f(\frac{R_3}{R_2+R_3})^2 A_{n,U3}^2 = 1.656 \times 10^{-14}V^2 \tag{22}$$

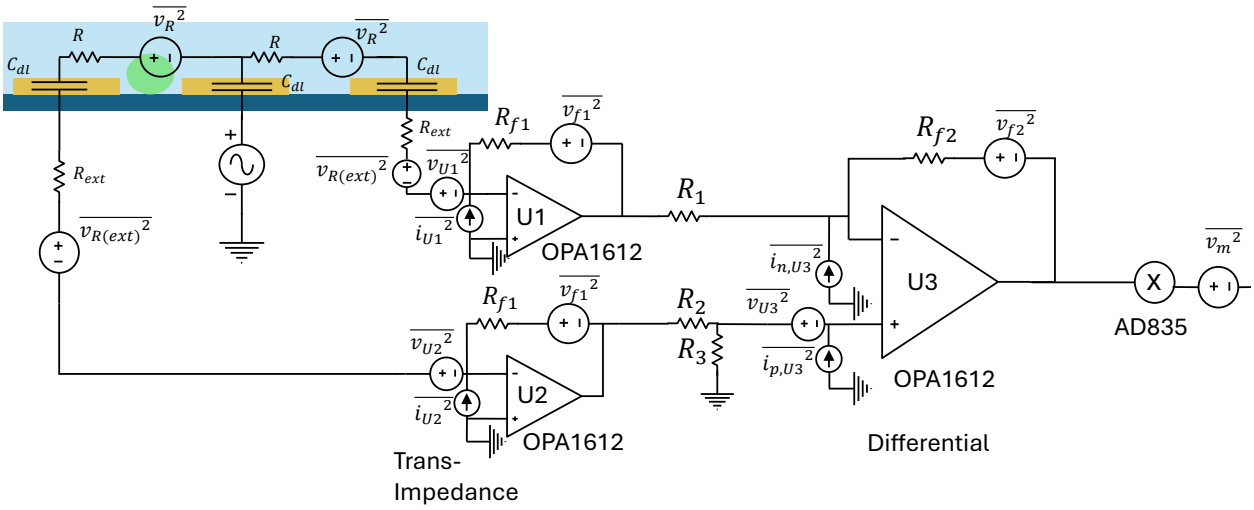

Fig. 2: Differential impedance flow cytometry equivalent circuit with noise sources.

$$\overline{v_{o,R_3}{}^2} = 4kT(R_3)\Delta f(\frac{R_2}{R_2+R_3})^2 A_{n,U3}^2 = 1.656\times10^{-14}V^2 \quad (23)$$

$$\overline{v_{o,U3}^2} = \overline{v_{U3}^2}A_{n,U3}^2 = 4.84\times10^{-18}V^2 \quad (24)$$

$$\overline{v_{o,i_n,U3}^2} = \overline{i_{n,U3}^2}R_{f2}^2 = 2.89\times10^{-18}V^2 \quad (25)$$

$$\overline{v_{o,i_p,U3}^2} = \overline{i_{p,U3}^2}(R_2||R_3)^2 A_{n,U3}^2 = 7.225\times10^{-19}V^2 \quad (26)$$

The resulting output voltage noise, combining all the current and previous sources, will just be the sum of all sources and can be represented as:

$$\overline{v_{o,tot}^2} = 2\overline{v_{o,U1}{}^2}+\overline{v_{o,R_{f2}}{}^2}+\overline{v_{o,R_1}{}^2}+\overline{v_{o,R_2}{}^2}+\overline{v_{o,U2}{}^2}+\overline{v_{o,R_3}{}^2}+\overline{v_{o,U3}^2}+\overline{v_{o,i_n,U3}^2}+\overline{v_{o,i_p,U3}^2} \approx 2.26\times10^{-6}V^2 \quad (27)$$

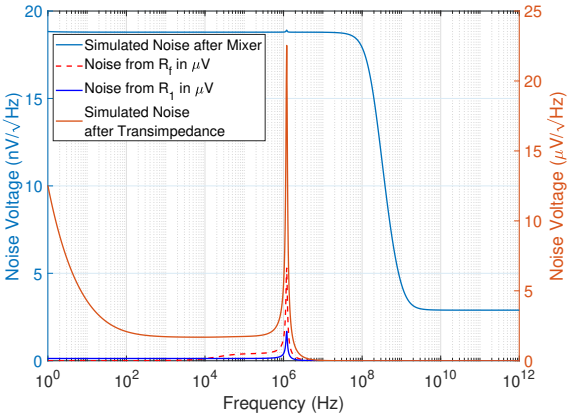

Fig. 3: Dual electrode system noise simulations at amplifier and mixer stages

III. Results and Discussion

The equivalent noise model circuits of the dual and differential electrodes impedance spectrometry systems are presented in Figs. 1 and 2 were simulated using the LTspice. The noise analysis was performed with a 10V input square wave signal of frequency 500 kHz. Fig. 3 shows the simulated output noise of the dual-electrode system at the amplifier and mixer stages along with the contribution of the noise from the feedback and input resistances R_f *and* $R+\Delta R$, respectively. The trans-impedance amplifier circuit exhibits higher output noise with an RMS value of $3mV$, which is close to the calculated value of $0.6mV$. From the simulation results, it can be observed that the feedback resistor and the input resistance introduced significant noise. This effect is mainly due to the higher values of the resistances, thus introducing higher thermal noise into the circuit output. It can also be observed that the output noise at the amplifier stage is the scaled version of the ratio of thermal noises of R_f *and* $R+\Delta R$, verifying that the gain amplifies the output noise. The noise contribution of the voltage mixer used in the impedance spectrometry for lock-in applications has been depicted with light blue graphs in Fig. 3. The magnitude of the noise introduced by the voltage mixer stage is in the order of nV, indicating that the mixer stage introduces minimal noise into the output of the system.

Similarly, the noise simulations were performed for the differential impedance spectrometry system. Fig. 4 (a) shows the noise simulation results at the differential amplifier stage and at the mixer output stage. The differential amplifier output stage exhibits higher output noise voltage with an RMS of $7mV$, which is comparable to the calculated noise voltage value of $1.5mV$. It was observed that the significant contribution towards the output voltage noise comes from the feedback resistors and the input resistors of higher magnitudes, as shown in Fig. 4 (b). As the electrical impedance spectrometry systems need to be robust and sensitive to the biological particles passing through the channel, it is recommended to have lower values of noise, preferably in the orders of nano volts. Since the bio-particles passing through the microfluidic channel produce a low voltage pulse. To reduce the noise in the impedance spectrometry systems, the solution resistances need to be reduced by modifying the channel geometry and using electrolytes with higher conductivity. It can be observed from Figs. 4 and 3 that a spike in noise voltage arises at frequency $\sim 1MHz$ having voltage noise of $\sim 70\mu V$ and $\sim 20\mu V$ in both cases respectively. The differential electrode system exhibits an RMS voltage noise of $\sim 640\mu V$ while the dual-electrode system exhibits $\sim 280\mu V$ in the frequency range of 3-10MHz. Suggesting the favorable operating bandwidth of the EIS system. Moreover, for better noise simulations, the experimentally estimated channel resistance would help produce better results and reduce the overall noise signature from the output of the amplifier. In future work, we aim to estimate the actual channel resistance along with improving the channel geometry, which will help in the reduction of the channel resistance.

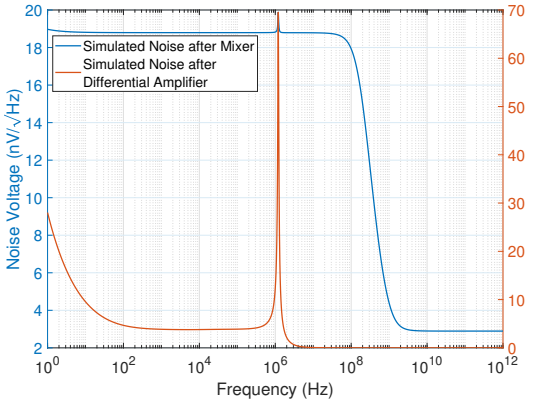

(a)

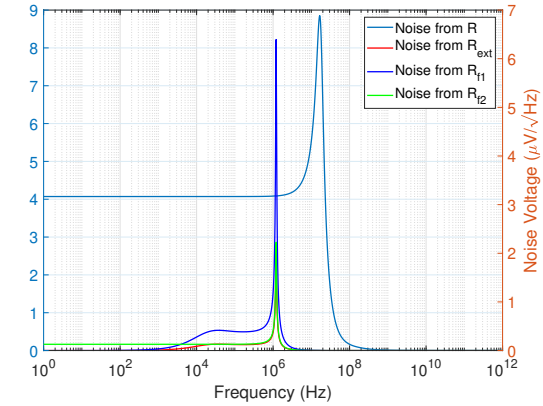

(b)

Fig. 4: (a) Triple electrode system noise simulations at amplifier and mixer stages. (b) Contribution of resistive elements to output noise.

IV. Conclusion

In this study, two configurations of the EIS system, dual-electrode and three-electrode (differential), were modeled and simulated using LTSpice for noise considerations. It was observed that the noise feedback resistors and estimated microfluidic channel resistances contribute significantly towards the total output voltage noise of the system. For the dual-electrode system, $0.6mV$ RMS value of output voltage noise was calculated over the frequency bandwidth of $1MHz$, while a noise RMS of $\sim 280\mu V$ was simulated over the frequency bandwidth of 3-10MHz. Similarly, for differential configurations, a noise RMS value of $1.5mV$ in $1MHz$ bandwidth was calculated as compared to the simulated value of $\sim 640\mu V$ over the frequency bandwidth of 3-10MHz. Understanding these frequency ranges and noise floors can help the designers select the most suitable input signal frequency and the bandwidth of output signal filters. In future work, we aim to explore the effect of active filtering on the noise outputs, estimate the actual channel resistance, and perform experiments to make comparisons with real-world data. We also aim to develop a deeper understanding of EIS architectures and perform a comparative analysis with existing architectures.

Acknowledgment

The authors acknowledges the funding support from U.S. National Science Foundation (Award No. 2329761), Rutgers School of Engineering, and Rutgers Global Health Institute.

REFERENCES

[1] A. Ramanavicius, A. Finkelsteinas, H. Cesiulis, and A. Ramanaviciene, "Electrochemical impedance spectroscopy of polypyrrole based electrochemical immunosensor," *Bioelectrochemistry*, vol. 79, no. 1, pp. 11–16, 2010. [Online]. Available: https://www.sciencedirect.com/science/article/pii/S1567539409002059

[2] J. A. Ribeiro and P. A. Jorge, "Applications of electrochemical impedance spectroscopy in disease diagnosis—a review," *Sensors and Actuators Reports*, vol. 8, p. 100205, 2024. [Online]. Available: https://www.sciencedirect.com/science/article/pii/S2666053924000213

[3] P. Arpaia, U. Cesaro, and N. Moccaldi, "Noninvasive measurement of transdermal drug delivery by impedance spectroscopy," *Scientific Reports*, vol. 7, no. 1, p. 44647, Mar 2017. [Online]. Available: https://doi.org/10.1038/srep44647

[4] S. Gawad, L. Schild, and P. Renaud, "Micromachined impedance spectroscopy flow cytometer for cell analysis and particle sizing," *Lab Chip*, vol. 1, pp. 76–82, 2001. [Online]. Available: http://dx.doi.org/10.1039/B103933B

[5] U. Hassan, T. Ghonge, B. Reddy Jr., M. Patel, M. Rappleye, I. Taneja, A. Tanna, R. Healey, N. Manusry, Z. Price, T. Jensen, J. Berger, A. Hasnain, E. Flaugher, S. Liu, B. Davis, J. Kumar, K. White, and R. Bashir, "A point-of-care microfluidic biochip for quantification of cd64 expression from whole blood for sepsis stratification," *Nature Communications*, vol. 8, no. 1, p. 15949, Jul 2017. [Online]. Available: https://doi.org/10.1038/ncomms15949

[6] H. Adam, S. C. Gopinath, T. Adam, M. A. Fakhri, E. T. Salim, and S. Subramaniam, "Exploring faradaic and non-faradaic electrochemical impedance spectroscopy approaches in parkinson's disease diagnosis," *Heliyon*, vol. 10, no. 5, Mar 2024. [Online]. Available: https://doi.org/10.1016/j.heliyon.2024.e27433

[7] R. Sengupta, H. Khand, and G. Sarusi, "Screening and diagnosis of respiratory diseases using metamaterial based sensitive terahertz impedance spectroscopy," *Sensing and Bio-Sensing Research*, vol. 44, p. 100639, 2024. [Online]. Available: https://www.sciencedirect.com/science/article/pii/S2214180424000217

[8] A. Keshtkar, A. Keshtkar, and R. H. Smallwood, "Electrical impedance spectroscopy and the diagnosis of bladder pathology," *Physiological Measurement*, vol. 27, no. 7, p. 585, apr 2006. [Online]. Available: https://dx.doi.org/10.1088/0967-3334/27/7/003

[9] A. Farooq, N. Z. Butt, and U. Hassan, "Circular shaped microelectrodes for single cell electrical measurements for lab-on-a-chip applications," *Biomedical Microdevices*, vol. 23, no. 3, p. 35, Jul 2021. [Online]. Available: https://doi.org/10.1007/s10544-021-00574-z

[10] D. Spencer, F. Caselli, P. Bisegna, and H. Morgan, "High accuracy particle analysis using sheathless microfluidic impedance cytometry," *Lab Chip*, vol. 16, pp. 2467–2473, 2016. [Online]. Available: http://dx.doi.org/10.1039/C6LC00339G

[11] K. Cheung, S. Gawad, and P. Renaud, "Impedance spectroscopy flow cytometry: On-chip label-free cell differentiation," *Cytometry Part A*, vol. 65A, no. 2, pp. 124–132, 2005. [Online]. Available: https://onlinelibrary.wiley.com/doi/abs/10.1002/cyto.a.20141

[12] C. Norton and U. Hassan, "Bioelectronic sensor with magnetic modulation to quantify phagocytic activity of blood cells employing machine learning," *ACS Sensors*, vol. 7, no. 7, pp. 1936–1945, Jul 2022. [Online]. Available: https://doi.org/10.1021/acssensors.2c00706

[13] B. K. Ashley, J. Sui, M. Javanmard, and U. Hassan, "Multi-modal sensing with integrated machine learning to differentiate specific leukocytes targeted by electrically sensitive hybrid particles," *Biosensors and Bioelectronics*, vol. 241, p. 115661, 2023. [Online]. Available: https://www.sciencedirect.com/science/article/pii/S0956566323006036

[14] C. Honrado, P. Bisegna, N. S. Swami, and F. Caselli, "Single-cell microfluidic impedance cytometry: from raw signals to cell phenotypes using data analytics," *Lab Chip*, vol. 21, pp. 22–54, 2021. [Online]. Available: http://dx.doi.org/10.1039/D0LC00840K

[15] B. Shen, J. Dawes, and M. L. Johnston, "A 10 mΩ, 50 khz-40 mhz impedance measurement architecture for source-differential flow cytometry," *IEEE Transactions on Biomedical Circuits and Systems*, vol. 16, no. 5, pp. 766–778, 2022.

[16] M. Tayyab, P. Xie, M. A. Sami, H. Raji, Z. Lin, Z. Meng, S. R. Mahmoodi, and M. Javanmard, "A portable analog front-end system for label-free sensing of proteins using nanowell array impedance sensors," *Scientific Reports*, vol. 12, no. 1, p. 20119, Nov 2022. [Online]. Available: https://doi.org/10.1038/s41598-022-23286-7

[17] P. Xie, X. Cao, Z. Lin, N. Talukder, S. Emaminejad, and M. Javanmard, "Processing gain and noise in multi-electrode impedance cytometers: Comprehensive electrical design methodology and characterization," *Sensors and Actuators B: Chemical*, vol. 241, pp. 672–680, 2017. [Online]. Available: https://www.sciencedirect.com/science/article/pii/S0925400516316124

[18] R. Subramanian and V. Lakshminarayanan, "A study of kinetics of adsorption of alkanethiols on gold using electrochemical impedance spectroscopy," *Electrochimica Acta*, vol. 45, no. 27, pp. 4501–4509, 2000. [Online]. Available: https://www.sciencedirect.com/science/article/pii/S0013468600005120

[19] R. W. DeBlois and C. P. Bean, "Counting and sizing of submicron particles by the resistive pulse technique," *Review of Scientific Instruments*, vol. 41, no. 7, pp. 909–916, 07 1970. [Online]. Available: https://doi.org/10.1063/1.1684724